Performance Evaluation of TOA Positioning in Asynchronous Cellular Networks Using Stochastic Geometry Models

Joe Khalife, *Student Member, IEEE*, Ceren Sevinç, *Student Member, IEEE*, and Zaher M. Kassas, *Senior Member, IEEE*

***Abstract*—Time-of-arrival (TOA) based positioning of a user equipment (UE) in asynchronous cellular networks is analyzed. Three different cases of prior knowledge of the UE clock bias statistics are considered. The squared-position error bound (SPEB) for each case is derived as a function of the ideal case SPEB: no UE or base station (BS) clock biases. Analytical relationships between the SPEB of the three studied cases are established. The cumulative density function (cdf) of the SPEB for each case is analyzed numerically via Monte Carlo simulations using stochastic geometry models.**

***Index Terms*—TOA positioning, 4G, 5G, stochastic geometry.**

I. Introduction

IN ORDER to keep up with the ever more stringent wireless localization requirements set by the Federal Communications Commission (FCC) [1], wireless providers enabled network-based positioning capabilities in 4G networks and aim to improve it in upcoming 5G networks. In a network-based approach, time-of-arrival (TOA) measurements made by neighboring base stations (BSs) on the user equipment (UE) are sent to a location server that estimates the UE position. Such approaches suffer from a number of drawbacks: (i) the user's privacy is compromised, since the UE location is revealed to the network even when there is no emergency, (ii) localization services are limited only to paying subscribers and from one cellular provider, and (iii) ambient cellular signals transmitted by other cellular providers are not exploited.

One promising technology that addresses these drawbacks and does not necessitate any change to the infrastructure is opportunistic navigation with cellular signals [2], [3]. While more BSs can be used for positioning in an opportunistic framework, the issue of synchronization must be resolved: one must account for UE and BS biases. This challenge has been addressed for opportunistic navigation by either (i) jointly estimating these biases with the UE state, which relies on UE motion and/or sensor fusion [3], [4], (ii) leveraging the relative frequency stability between BSs [5], [6], or (iii) through the use of a reference receiver [7]. Moreover, several experiments have demonstrated indoor and outdoor navigation with such signals [8]–[10]. In the aforementioned work, opportunistic positioning with cellular signals has been studied for a deterministic realization of the BS positions [11].

Instead of deterministic network modeling techniques, stochastic geometry has been widely adopted over the last decade to model the location of BSs for several reasons [12], [13]: (i) modeling BS locations with point processes captures the randomness of BS deployment and (ii) stochastic geometry approach brings analytically tractable results. These perks of stochastic geometry sparked studies to characterize the localization performance in wireless networks [14], [15]. In [16], a cellular network model with a homogeneous Poisson point process (PPP) was used to derive bounds for TOA-based positioning, while the effect of signal-to-noise ratio (SNR) heterogeneity in TOA-based localization was studied in [17] by using a binomial point process (BPP) model. Such analyses shed some light on the expected localization performance in 4G and sub 6-GHz 5G networks; however, they make the *impractical* assumption that the UE and BSs are synchronized.

This letter aims to analyze the performance of positioning in cellular systems using stochastic geometry models. The approach employed in this letter follows the one in the literature on TOA-performance characterization in wireless networks with the added complexity of accounting for UE and BS clock biases. To this end, three cases of prior knowledge on the UE clock bias statistics are explored: (i) the UE knows its clock bias statistics, (ii) the UE does not know its clock bias statistics but jointly estimates its position and clock bias, and (iii) the UE does not know its clock bias statistics nor is estimating its clock bias. The third case arises when the methods proposed in the literature that assume synchronization are used in a realistic system, resulting in an estimator with mismatched prior statistics. It is shown in this letter that this has a drastic negative effect on the performance. Similar to the rest of the literature, the squared-position error bound (SPEB) metric is evaluated for each case.

The remainder of this letter is organized as follows. Section II describes the BS position and TOA measurement models. Section III presents the positioning cases, characterizes their corresponding SPEBs, and establishes relationships between the SPEBs. Section IV provides numerical simulation results evaluating the cumulative density function (cdf) of the SPEBs and validating the established relationships. Concluding remarks are given in Section V.

Notation: Lower-case bold variables (e.g., $\boldsymbol{x}$) indicate column vectors and upper-case bold variables (e.g., $\mathbf{X}$) indicate

Manuscript received March 15, 2020; revised April 28, 2020; accepted April 30, 2020. Date of publication May 6, 2020; date of current version September 9, 2020. This work was supported in part by the National Science Foundation under Grant 1929571 and Grant 1929965, and in part by the Office of Naval Research under Grant N00014-19-1-2511. The associate editor coordinating the review of this article and approving it for publication was Y. Shen. *(Corresponding author: Zaher M. Kassas.)*

Joe Khalife is with the Mechanical and Aerospace Engineering Department, University of California at Irvine, Irvine, CA 92697 USA (e-mail: khalifej@uci.edu).

Ceren Sevinç is with the Electrical and Computer Engineering Department, University of California at Riverside, Riverside, CA 92521 USA (e-mail: csevinc@ee.ucr.edu).

Zaher M. Kassas is with the Mechanical and Aerospace Engineering Department, University of California at Irvine, Irvine, CA 92697 USA, and also with the Electrical Engineering and Computer Science Department, University of California at Irvine, Irvine, CA 92697 USA (e-mail: zkassas@ieee.org).

Digital Object Identifier 10.1109/LWC.2020.2992742

matrices. The symbol $\mathbf{I}_N$ denotes the $N \times N$ identity matrix and $\mathbf{1}_N$ the $N \times 1$ vector of ones. The diagonal matrix whose elements are $x_1, \ldots, x_N$ is denoted $\mathrm{diag}\,[x_1, \ldots, x_N]$. Also, let $p(\boldsymbol{z}; \boldsymbol{x})$ be the probability distribution of $\boldsymbol{z}$ parameterized by $\boldsymbol{x}$, and $\mathcal{N}(\boldsymbol{z}; \boldsymbol{x}, \boldsymbol{\Sigma})$ the multivariate Gaussian distribution of the random vector $\boldsymbol{z}$ with mean $\boldsymbol{x}$ and covariance $\boldsymbol{\Sigma}$.

II. System Model

In the following, let $\boldsymbol{p}_{\mathrm{UE}} \triangleq [x_{\mathrm{UE}}, y_{\mathrm{UE}}]^{\mathsf{T}}$ denote the UE's two-dimensional (2–D) position and $\boldsymbol{p}_{\mathrm{BS}_n} \triangleq [x_{\mathrm{BS}_n}, y_{\mathrm{BS}_n}]^{\mathsf{T}}$ denote the *n*-th BS's 2–D position, where $n = 1, \ldots, N$, and *N* is the total number of available BSs. The TOA measurement made by the UE on the *n*-th BS, expressed in meters, can be parameterized as

$$z_n = d_n + c \cdot [\delta t_{\mathrm{UE}} - \delta t_{\mathrm{BS}_n}] + v_n, \tag{1}$$

where $d_n \triangleq \left\| \boldsymbol{p}_{\mathrm{UE}} - \boldsymbol{p}_{\mathrm{BS}_n} \right\|_2$, δt_{UE} and δt_{BS_n} are the UE's and the *n*-th BS's clock biases, respectively, and v_n is the measurement noise, which is modeled as a zero-mean Gaussian random variable with variance σ_n^2. Several models of σ_n^2 as a function of the signal-to-noise ratio, distance, bearing angle, signal bandwidth, etc. were established [18]. In this letter, it is assumed that the direct path (DP) does not overlap with other multipath components. In this case, the DP is resolvable and the overall signal boils down to a signal that is composed of the DP only for positioning, thereby attaining its maximum accuracy. Therefore, assuming limited interference between BSs, σ_n^2 is modeled as

$$\sigma_n^2 = \frac{c^2}{8\pi^2\beta^2} \left(\frac{d_n}{d_{\min}} \right)^{\alpha} \frac{1}{S/N_0},$$

where β is the effective signal bandwidth, α is the path-loss exponent, *S* is the transmitted signal power, and N_0 is the power spectral density of the additive white Gaussian channel noise [17]. Moreover, it is assumed that $\delta t_{\mathrm{UE}} \sim \mathcal{N}(0, \sigma^2_{\delta t_{\mathrm{UE}}})$, $\delta t_{\mathrm{BS}_n} \sim \mathcal{N}(0, \sigma^2_{\delta t_{\mathrm{BS}}})$, and v_n and v_m are uncorrelated for $n \neq m$. Note that the clock bias may also be modeled as a constant clock offset and a clock skew [19]. However, this letter characterizes single snapshot positioning; hence, only the clock offset is considered. Equation (1) can be written in vector form as

$$\begin{aligned} \boldsymbol{z}_N &= \boldsymbol{d}_N + c\delta t_{\mathrm{UE}} \mathbf{1}_N - c\boldsymbol{\delta t}_{\mathrm{BS}_N} + \boldsymbol{v}_N, \\ \boldsymbol{z}_N &\triangleq [z_1, \ldots, z_N]^{\mathsf{T}}, \qquad \boldsymbol{d}_N \triangleq [d_1, \ldots, d_N]^{\mathsf{T}}, \\ \boldsymbol{\delta t}_{\mathrm{BS}_N} &\triangleq \left[\delta t_{\mathrm{BS}_1}, \ldots, \delta t_{\mathrm{BS}_N}\right]^{\mathsf{T}}, \quad \boldsymbol{v}_N \triangleq [v_1, \ldots, v_N]^{\mathsf{T}}. \end{aligned}$$

Furthermore, define the following quantities

$$\begin{aligned} \boldsymbol{\Sigma}_v &\triangleq \mathrm{cov}[\boldsymbol{v}_N] = \mathrm{diag}\left[\sigma_1^2, \ldots, \sigma_N^2\right], \\ \boldsymbol{\Sigma}_{\delta t_{\mathrm{BS}}} &\triangleq \mathrm{cov}\left[\boldsymbol{\delta t}_{\mathrm{BS}_N}\right] = \sigma^2_{\delta t_{\mathrm{BS}}} \mathbf{I}_N, \quad \boldsymbol{\Sigma}_{\delta t_{\mathrm{UE}}} \triangleq \sigma^2_{\delta t_{\mathrm{UE}}} \mathbf{1}_N \mathbf{1}_N^{\mathsf{T}}. \end{aligned}$$

III. UE Positioning Cases and SPEB Characterization

This section analyzes three positioning cases and the SPEB is formulated for each case.

A. UE Positioning Cases

Consider the following three cases with different UE prior knowledge about its clock bias statistics:

Case I: The UE is estimating its position only and knows the statistics of its own and the BSs' clock biases. Hence, the parameter $\boldsymbol{\theta}_I$ and the likelihood function $p_I(\boldsymbol{z}; \boldsymbol{\theta}_I)$ associated with this case are defined as

$$\boldsymbol{\theta}_I \triangleq \boldsymbol{p}_{\mathrm{UE}}, \quad p_I(\boldsymbol{z}; \boldsymbol{\theta}_I) = \mathcal{N}(\boldsymbol{z}; \boldsymbol{d}, \boldsymbol{\Sigma}_I), \tag{2}$$

where $\boldsymbol{\Sigma}_I \triangleq \boldsymbol{\Sigma}_v + c^2 \boldsymbol{\Sigma}_{\delta t_{\mathrm{BS}}} + c^2 \boldsymbol{\Sigma}_{\delta t_{\mathrm{UE}}}$.

Case II: The UE is jointly estimating its position and clock bias and knows the statistics of the BSs' clock biases only. Hence, the parameter $\boldsymbol{\theta}_{II}$ and the likelihood function $p_{II}(\boldsymbol{z}; \boldsymbol{\theta}_{II})$ associated with this case are defined as

$$\boldsymbol{\theta}_{II} \triangleq \left[\boldsymbol{p}_{\mathrm{UE}}^{\mathsf{T}}, \delta t_{\mathrm{UE}}\right]^{\mathsf{T}}, \; p_{II}(\boldsymbol{z}; \boldsymbol{\theta}_{II}) = \mathcal{N}(\boldsymbol{z}; \boldsymbol{\rho}, \boldsymbol{\Sigma}_{II}), \tag{3}$$

where $\boldsymbol{\rho} \triangleq \boldsymbol{d} + c\delta t_{\mathrm{UE}} \mathbf{1}_N$ and $\boldsymbol{\Sigma}_{II} \triangleq \boldsymbol{\Sigma}_v + c^2 \boldsymbol{\Sigma}_{\delta t_{\mathrm{BS}}}$.

Case III: The UE is estimating its position only, knows the statistics of the BSs' clock biases, and assumes the UE is synchronized with the system, i.e., δt_{UE} is assumed to be zero, which is not necessarily true. Hence, the parameter $\boldsymbol{\theta}_{III}$ and the likelihood function $p_{III}(\boldsymbol{z}; \boldsymbol{\theta}_{III})$ associated with this case are defined similarly to Case I as

$$\boldsymbol{\theta}_{III} \triangleq \boldsymbol{\theta}_I, \quad p_{III}(\boldsymbol{z}; \boldsymbol{\theta}_{III}) = p_I(\boldsymbol{z}; \boldsymbol{\theta}_I). \tag{4}$$

Remark 1: The main difference between Case I and Case III is that the UE assumes its bias is zero; hence, the CRLB of Case I cannot be achieved in Case III. This assumption is often made in the TOA localization literature and the goal of this letter is to show the drastic effect of this assumption. To study Case III, an estimator that achieves the CRLB in the absence of UE clock bias, i.e., Case I with $\sigma^2_{\delta t_{\mathrm{UE}}} = 0$, is applied and its MSE is studied. The cases are summarized in Table I.

TABLE I
Summary of UE Positioning Cases

Case	Estimated states	Statistics known	Model mismatch
I	$\boldsymbol{p}_{\mathrm{UE}}$	$\sigma_{\delta t_{\mathrm{BS}}}, \sigma_{\delta t_{\mathrm{UE}}}$	None
II	$\boldsymbol{p}_{\mathrm{UE}}, \delta t_{\mathrm{UE}}$	$\sigma_{\delta t_{\mathrm{BS}}}$	None
III	$\boldsymbol{p}_{\mathrm{UE}}$	$\sigma_{\delta t_{\mathrm{BS}}}$	$\delta t_{\mathrm{UE}} \equiv 0$

B. SPEB General Definition

The position mean squared error (MSE) of any estimator will be lower-bounded according to MSE $\geq$ SPEB. In this letter, maximum likelihood estimators (MLEs) are used to estimate the UE position and/or clock bias from TOA measurements. Such MLEs will closely approach the Cramer-Rao lower bound (CRLB), with small differences due to linearization errors. For estimators that achieve the CRLB, the position MSE becomes the SPEB; hence the choice of SPEB as a performance metric to be studied. It is important to note that the purpose of this letter is not to obtain an analytical expression of the distribution of the SPEB, but explicitly express the SPEB as a function of random variables whose distributions are known and have been validated (e.g., bearing angles and distances between the UE and BSs). In addition to the fact that obtaining analytical expressions is intractable, such analysis would require a rigorous treatment that cannot fit into this letter. Instead, this letter aims to characterize through Monte Carlo simulations the SPEB of the three different aforementioned cases and to draw key observations. Moreover, this letter aims to compare analytically the SPEBs of each cases

in a deterministic sense, i.e., for a given BPP realization. The SPEB for each case is defined as [20]

$$\mathrm{SPEB} \triangleq \mathrm{trace}\left\{\left[\left(\boldsymbol{\mathcal{I}}(\boldsymbol{\theta})\right)^{-1}\right]_{2\times 2}\right\},$$

where $\boldsymbol{\mathcal{I}}(\boldsymbol{\theta})$ is the Fisher information matrix (FIM) of parameter $\boldsymbol{\theta}$ and $[\mathbf{A}]_{2\times 2}$ indicates the upper 2×2 diagonal block of matrix $\mathbf{A}$. In the case of the FIM, this block corresponds to the two position parameters.

1) SPEB for Case I: From $p_I(\boldsymbol{z};\boldsymbol{\theta}_I)$, the FIM for Case I can be shown to be

$$\boldsymbol{\mathcal{I}}(\boldsymbol{\theta}_I) = \mathbf{G}^{\mathsf{T}}\Sigma_I^{-1}\mathbf{G}, \quad \mathbf{G} \triangleq \begin{bmatrix}\cos\phi_1,\ldots,\cos\phi_N \\ \sin\phi_1,\ldots,\sin\phi_N\end{bmatrix}^{\mathsf{T}},$$

where ϕ_n is the *n*-th BS's bearing angle, and the SPEB is given by

$$\mathrm{SPEB}_I = \mathrm{trace}\left[\left(\mathbf{G}^{\mathsf{T}}\boldsymbol{\Sigma}_I^{-1}\mathbf{G}\right)^{-1}\right].$$

It is worth mentioning that SPEB_I is achievable. A weighted nonlinear least-squares (WNLS) estimator with weighting matrix $\boldsymbol{\Sigma}_I^{-1}$, which is the MLE of $\boldsymbol{\theta}_I$, can achieve $SPEB_I$.

2) SPEB for Case II: From $p_{II}(\boldsymbol{z};\boldsymbol{\theta}_{II})$, the FIM for Case II can be shown to be

$$\boldsymbol{\mathcal{I}}(\boldsymbol{\theta}_{II}) = \mathbf{H}^{\mathsf{T}}\boldsymbol{\Sigma}_{II}^{-1}\mathbf{H}, \quad \mathbf{H} = [\mathbf{G}\ \mathbf{1}_N].$$

Using block matrix inversion, the SPEB for Case II can be shown to be

$$\mathrm{SPEB}_{II} = \mathrm{trace}\left[\left(\mathbf{G}^{\mathsf{T}}\boldsymbol{\Psi}_{II}\mathbf{G}\right)^{-1}\right],$$
$$\boldsymbol{\Psi}_{II} = \boldsymbol{\Sigma}_{II}^{-1} - \frac{\boldsymbol{\Sigma}_{II}^{-1}\mathbf{1}_N\mathbf{1}_N^{\mathsf{T}}\boldsymbol{\Sigma}_{II}^{-1}}{\mathbf{1}_N^{\mathsf{T}}\boldsymbol{\Sigma}_{II}^{-1}\mathbf{1}_N}.$$

Similarly to Case I, a WNLS estimator with weighting matrix $\boldsymbol{\Sigma}_{II}^{-1}$ is the MLE of $\boldsymbol{\theta}_{II}$ and can achieve $SPEB_{II}$. Note that not knowing the statistics of δt_{UE} is equivalent to having a diffuse prior.

3) SPEB for Case III: The CRLB in Case III cannot be achieved because of the model mismatch. Therefore, instead of SPEB, the MSE of a WNLS with weighting matrix $\boldsymbol{\Sigma}_{II}^{-1}$ estimating the UE position is used to characterize Case III. This case arises when the estimator assumes full synchronization of the UE with the network. Instead of using MSE_{III}, the $SPEB_{III}$ notation is abused in order to keep the notation consistent with $SPEB_I$ and $SPEB_{II}$. Subsequently, $SPEB_{III}$ can be shown to be

$$\mathrm{SPEB}_{III} = \mathrm{trace}\left[\mathbf{K}\boldsymbol{\Sigma}_{III}\mathbf{K}^{\mathsf{T}}\right],$$

where $\mathbf{K} \triangleq (\mathbf{G}^{\mathsf{T}}\boldsymbol{\Sigma}_{II}^{-1}\mathbf{G})^{-1}\mathbf{G}^{\mathsf{T}}\boldsymbol{\Sigma}_{II}^{-1}$ and $\boldsymbol{\Sigma}_{III} \triangleq \boldsymbol{\Sigma}_I$.

C. Performance Comparison

First, define SPEB_0 as the SPEB where there is no UE clock bias, which is the case often assumed in the literature. This SPEB can be expressed as

$$\mathrm{SPEB}_0 = \mathrm{trace}\left[\left(\mathbf{G}^{\mathsf{T}}\boldsymbol{\Sigma}_{II}^{-1}\mathbf{G}\right)^{-1}\right].$$

The following three lemmas establish relationships between the SPEB for each case and $SPEB_0$.

Lemma 1: The SPEB for Case I can be expressed as

$$\mathrm{SPEB}_I = \mathrm{SPEB}_0 + \frac{c^2\sigma_{\delta t_{\mathrm{UE}}}^2}{1 + c^2\sigma_{\delta t_{\mathrm{UE}}}^2\gamma^2}\kappa^2, \tag{5}$$

for some $\kappa^2 \geq 0$ and $\gamma^2 > 0$ that are functions of the BSs' positions and $\boldsymbol{\Sigma}_{II}$.

Proof: Using the matrix inversion lemma, $\boldsymbol{\Sigma}_I^{-1}$ may be expressed as

$$\boldsymbol{\Psi}_I \triangleq \boldsymbol{\Sigma}_I^{-1} = \boldsymbol{\Sigma}_{II}^{-1} - \frac{c^2\sigma_{\delta t_{\mathrm{UE}}}^2\boldsymbol{\Sigma}_{II}^{-1}\mathbf{1}_N\mathbf{1}_N^{\mathsf{T}}\boldsymbol{\Sigma}_{II}^{-1}}{1 + c^2\sigma_{\delta t_{\mathrm{UE}}}^2\left(\mathbf{1}_N^{\mathsf{T}}\boldsymbol{\Sigma}_{II}^{-1}\mathbf{1}_N\right)}.$$

Using the matrix inversion lemma again, it can be shown that

$$\left(\mathbf{G}^{\mathsf{T}}\boldsymbol{\Sigma}_I^{-1}\mathbf{G}\right)^{-1} = \left(\mathbf{G}^{\mathsf{T}}\boldsymbol{\Sigma}_{II}^{-1}\mathbf{G}\right)^{-1} + \frac{\mathbf{K}\mathbf{1}_N\mathbf{1}_N^{\mathsf{T}}\mathbf{K}^{\mathsf{T}}}{\frac{1}{c^2\sigma_{\delta t_{\mathrm{UE}}}^2} + \mathbf{1}_N^{\mathsf{T}}\boldsymbol{\Psi}_0\mathbf{1}_N}, \tag{6}$$

where $\boldsymbol{\Psi}_0 \triangleq \boldsymbol{\Sigma}_{II}^{-1} - \boldsymbol{\Sigma}_{II}^{-1}\mathbf{G}(\mathbf{G}^{\mathsf{T}}\boldsymbol{\Sigma}_{II}^{-1}\mathbf{G})^{-1}\mathbf{G}^{\mathsf{T}}\boldsymbol{\Sigma}_{II}^{-1}$. The matrix $\boldsymbol{\Psi}_0$ may be expressed as

$$\boldsymbol{\Psi}_0 = \boldsymbol{\Sigma}_{II}^{-\frac{1}{2}}\mathbf{P}\boldsymbol{\Sigma}_{II}^{-\frac{1}{2}},$$

where $\boldsymbol{\Sigma}_{II}^{-\frac{1}{2}}$ is a square-root of $\boldsymbol{\Sigma}_{II}^{-1}$ and $\mathbf{P} \triangleq \mathbf{I}_N - \boldsymbol{\Sigma}_{II}^{-\frac{1}{2}}\mathbf{G}(\mathbf{G}^{\mathsf{T}}\boldsymbol{\Sigma}_{II}^{-1}\mathbf{G})^{-1}\mathbf{G}^{\mathsf{T}}\boldsymbol{\Sigma}_{II}^{-\frac{1}{2}}$ is an idempotent orthogonal projection matrix, i.e., $\mathbf{PP} = \mathbf{P}$. Subsequently, the quadratic form $\mathbf{1}_N^{\mathsf{T}}\boldsymbol{\Psi}_0\mathbf{1}_N$ may be expressed as

$$\mathbf{1}_N^{\mathsf{T}}\boldsymbol{\Psi}_0\mathbf{1}_N = \mathbf{1}_N^{\mathsf{T}}\boldsymbol{\Sigma}_{II}^{-\frac{1}{2}}\mathbf{P}\mathbf{P}\boldsymbol{\Sigma}_{II}^{-\frac{1}{2}}\mathbf{1}_N = \left\|\mathbf{P}\boldsymbol{\Sigma}_{II}^{-\frac{1}{2}}\mathbf{1}_N\right\|_2^2 \triangleq \gamma^2.$$

It is important to note that although $\|\mathbf{P}\boldsymbol{\Sigma}_{II}^{-\frac{1}{2}}\mathbf{1}_N\|_2^2 \geq 0$, it is assumed for simplicity that the trivial case is never achieved; hence $\gamma^2 > 0$. Taking the trace of (6), using the linear and cyclic properties of the matrix trace, and defining $\kappa^2 \triangleq \|\mathbf{K}\mathbf{1}_N\|_2^2$, (5) is deduced. ∎

Lemma 2: The SPEB for Case II does not depend on $\sigma_{\delta t_{\mathrm{UE}}}^2$ and can be expressed as

$$\mathrm{SPEB}_{II} = \mathrm{SPEB}_0 + \frac{1}{\gamma^2}\kappa^2. \tag{7}$$

Proof: The proof of Lemma 2 follows the same steps as in Lemma 1, for the same values of γ^2 and κ^2 defined earlier. ∎

It is important to note that since SPEB_{II} does not depend on $\sigma_{\delta t_{\mathrm{UE}}}^2$, accurate positioning is possible in Case II even when $\sigma_{\delta t_{\mathrm{UE}}}^2$ is very large.

Lemma 3: The SPEB for Case III can be expressed as

$$\mathrm{SPEB}_{III} = \mathrm{SPEB}_0 + c^2\sigma_{\delta t_{\mathrm{UE}}}^2\kappa^2. \tag{8}$$

Proof: The proof of Lemma 3 follows the same steps as in Lemma 1, for the same value of κ^2 defined earlier. ∎

The lemmas stated above expose the relationships between the SPEBs of each case. It can be seen that

$$\mathrm{SPEB}_I \leq \mathrm{SPEB}_{II}, \quad \mathrm{SPEB}_I \leq \mathrm{SPEB}_{III}\,.$$

At the limits of $c^2\sigma_{\delta t_{\mathrm{UE}}}^2$, the following can be observed

$$\lim_{\sigma_{\delta t_{\mathrm{UE}}}^2\to\infty} \mathrm{SPEB}_I = \mathrm{SPEB}_{II},$$
$$\lim_{\sigma_{\delta t_{\mathrm{UE}}}^2\to 0} \mathrm{SPEB}_I = \lim_{\sigma_{\delta t_{\mathrm{UE}}}^2\to 0} \mathrm{SPEB}_{III} = \mathrm{SPEB}_0\,.$$

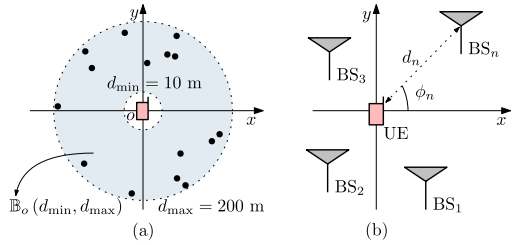

Fig. 1. (a) BPP realization with $N = 15$. (b) Parametrization of the n-th BS position by its range d_n and bearing angle ϕ_n to the UE.

One interesting observation is that Case III is not always worse than Case II, and the direction of the inequality depends on: (i) $\frac{1}{\gamma^2}$ in $SPEB_{II}$, which captures the loss of information from $\boldsymbol{z}_N$ on $\boldsymbol{p}_{\rm UE}$ due to estimating more parameters, and (ii) $c^2\sigma^2_{\delta t_{\rm UE}}$ in $SPEB_{III}$, which captures the effect of an additional error in the measurement since $\delta t_{\rm UE}$ is not necessarily zero. Stated in words, this result is somewhat counter-intuitive: in some cases, when $\sigma^2_{\delta t_{\rm UE}}$ is unknown, ignoring the existence of the UE bias yields better performance than jointly estimating it with the UE position, which implies that a biased estimator of the UE position can yield a lower MSE than an unbiased one. E.g., for $N = 4$, $\{\phi_n\}_{n=1}^4 = \{10^\circ, 175^\circ, 250^\circ, 330^\circ\}$, $\boldsymbol{\Sigma}_{II} = 4\mathbf{I}_4$ m^2, and $c^2\sigma^2_{\delta t_{\rm UE}} = 16$ m^2, then $SPEB_I \approx 22.1$ m^2, $SPEB_{II} \approx 44$ m^2, and $SPEB_{III} \approx 37$ m^2. Practically, $c^2\sigma^2_{\delta t_{\rm UE}} \gg \frac{1}{\gamma^2}$, hence ${\rm SPEB}_{II}$ is usually lower than ${\rm SPEB}_{III}$.

Recall that a WNLS estimator with weighting matrix $\boldsymbol{\Sigma}_I^{-1}$ closely approaches $SPEB_I$ when $\sigma^2_{\delta t_{\rm UE}}$ is known, with small differences due to linearization errors. Therefore, the aforementioned WNLS estimator, although not explicitly formulated as such, is equivalent to a WNLS estimating the UE clock bias when $\sigma^2_{\delta t_{\rm UE}}$ is very large. E.g., using the same parameters of the previous example but setting $c^2\sigma^2_{\delta t_{\rm UE}} = 10^{10}$ m^2 yields $SPEB_I \approx SPEB_{II} \approx 44$ m^2 and $SPEB_{III} \approx 2.06 \times 10^{10}$ m^2. In contrast, when $\sigma^2_{\delta t_{\rm UE}}$ is zero, there will be a constant "loss of information" between Case I and Case II since the latter is trying to estimate a non-existing quantity.

IV. Numerical Analysis

This section presents the BS position model and Monte Carlo simulation results to numerically analyze the cdf of the SPEBs in an asynchronous cellular network. For each Monte Carlo simulation, 10^5 realizations of the SPEB are generated to calculate the cdf.

A. BS Position Model

The BS network is modeled as a BPP, where $N \geq 3$ BSs are independently and uniformly distributed over an annular region centered at the origin o, i.e., $\mathbb{B}_o(d_{\min}, d_{\max}) = \pi(d^2_{\max} - d^2_{\min})$ [17], where $d_{\min}$ is the minimum distance required for the far-field assumption to hold and $d_{\max}$ is the maximum distance for which ranging signals can be detected by the receiver (see Fig. 1(a) for $N = 15$). The location of the n-th BS is represented by (d_n, ϕ_n), as shown in Fig. 1(b).

B. Numerical Analysis Settings

The path-loss exponent was chosen to be $\alpha = 3.7$ to characterize the path-loss in deep urban and indoor environments and the number of BSs was varied between 4, 6, 8, and 10. The Monte Carlo simulation parameters are shown in Table II. The 3GPP2 protocol requires BS clock biases to be bounded by $\epsilon \sim 3\mu$s [21]. Assuming the BS clock biases to be uniformly distributed between $-\epsilon$ and ϵ, a moment matching method can be used to approximate a Gaussian pdf for $\delta t_{{\rm BS}_n}$ in order to maintain the Gaussian assumption in the analysis, leading to the values in Table II. The UE clock bias was chosen similarly. Although there are no synchronization requirements for the UE, UEs will get timing information from the servicing BS and synchronize to it. Therefore, reasonably small values of the UE clock bias are considered in the numerical analysis.

TABLE II
Parameter Values for Monte Carlo Simulations

Parameter	Value/Assumption
N (number of BSs)	4, 6, 8, 10
α (path-loss exponent)	3.7
S/N_0	60 dB
$(d_{\min}, d_{\max})$	(10 m, 200 m)
β (effective bandwidth)	100 MHz

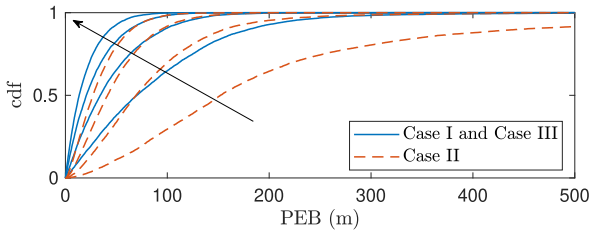

Fig. 2. Cdf of ${\rm PEB}_I = {\rm PEB}_{III}$ and ${\rm PEB}_{II}$ in the absence of UE and BS clock biases for $N = 4$, 6, 8, and 10. The black arrow indicates the direction of change of the cdf as N increases.

C. Numerical Results

Numerical results are provided next for several simulation scenarios. Note that the cdf of the ${\rm PEB} = \sqrt{\rm SPEB}$ is provided for a more intuitive visualization.

1) Best Case Scenario: Perfectly Synchronized Network: The best case scenario is provided for comparison purposes. In this scenario, the UE and BS clock biases are assumed to be zero, i.e., perfectly synchronized UE-BS network. Note that in this scenario, Cases I and III will perform similarly and Case II is expected to perform worse. The results for all cases are shown in Fig. 2 for $N = 4$, 6, 8, and 10.

2) Effect of BS Clock Biases: Next, the effect of BS clock biases is evaluated by setting $N = 8$ and $\sqrt{3}\sigma_{\delta t_{UE}} = 1\mu$s, and $\sigma_{\delta t_{BS}}$ was varied. The results are shown in Fig. 3. The effect of BS clock bias can be seen by comparing Figs. 2 and 3: all the cdfs are shifted to the right. Moreover, Fig. 3 shows that as $\sigma_{\delta t_{BS}}$ decreases and $\sigma_{\delta t_{UE}}$ becomes more dominant, Cases I and II still improve significantly but Case III almost saturates since the UE bias is taking over.

3) Effect of UE Clock Biases: Next, the effect of UE clock bias is evaluated by setting $N = 8$ and $\sqrt{3}\sigma_{\delta t_{BS}} = 0.25\mu$s, and $\sigma_{\delta t_{UE}}$ was varied. The results are shown in Fig. 4. Fig. 4 shows how sensitive Case III is to the UE clock bias, while, as expected, the cdf of ${\rm PEB}_{II}$ does not change with $\sigma_{\delta t_{UE}}$. When $\sigma_{\delta t_{UE}}$ becomes very small, Cases I and III coincide, also as expected. The key takeaway from Fig. 4 is the importance of estimating the UE clock bias, even if some performance may be sacrificed. For large values of $\sigma_{\delta t_{UE}}$, ${\rm PEB}_{II}$ is significantly

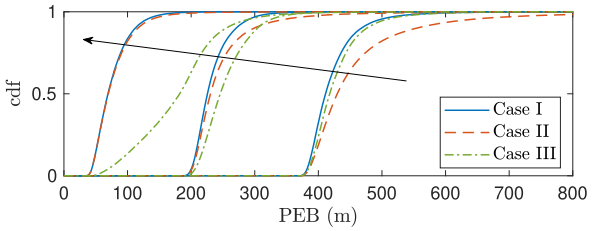

Fig. 3. Cdf of PEB_I, PEB_{II} and PEB_{III} for $N = 8$, $\sqrt{3}\sigma_{\delta t_{UE}} = 1$ μs and $\sqrt{3}\sigma_{\delta t_{BS}} = 0.25$, 1.5, and 3 μs. The black arrow indicates the direction of change of the cdf as $\sigma_{\delta t_{BS}}$ decreases.

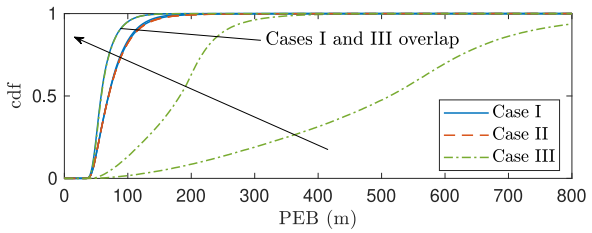

Fig. 4. Cdf of PEB_I, PEB_{II} and PEB_{III} for $N = 8$, $\sqrt{3}\sigma_{\delta t_{BS}} = 0.25$ μs and $\sqrt{3}\sigma_{\delta t_{UE}} = 0.1$, 1, and 3 μs. The black arrow indicates the direction of change of the cdf as $\sigma_{\delta t_{UE}}$ decreases.

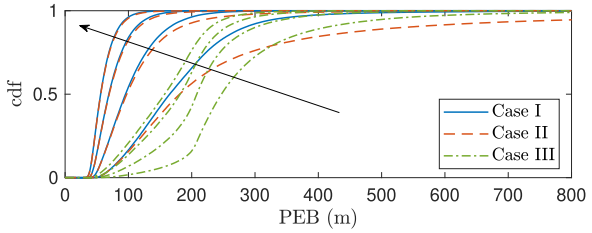

Fig. 5. Cdf of PEB_I, PEB_{II} and PEB_{III} for $\sqrt{3}\sigma_{\delta t_{BS}} = 0.25$ μs, $\sqrt{3}\sigma_{\delta t_{UE}} = 1$ μs and $N = 4$,6,8, and 10. The black arrow indicates the direction of change of the cdf as N increases.

smaller than PEB_{III}, while PEB_{III} is slightly smaller than PEB_{II} when $\sigma_{\delta t_{UE}}$ is small.

4) Effect of Number of BSs: Next, the effect of N is evaluated. To this end, $\sqrt{3}\sigma_{\delta t_{BS}}$ was fixed to 0.25 μs, $\sqrt{3}\sigma_{\delta t_{UE}}$ to 1 μs, and N was varied. The results are shown in Fig. 5.

Fig. 5 shows the intuitive result of the performance improving as N increases. It was noticed that the PEB is decreasing at a much slower rate than in the absence of biases, as can be seen by comparing Fig. 5 to Fig. 2. This reduction is due to the tradeoff that comes with adding more BSs: improvement in the UE-BS geometry at the cost of additional biases.

V. Conclusion

This letter evaluated the SPEB of UE positioning in asynchronous 4G and sub-6 GHz 5G networks for three cases: (i) the UE bias statistics are known and only the UE position is estimated, (ii) the UE bias statistics are unknown and the UE jointly estimates its position and clock bias, and (iii) the UE clock bias statistics are unknown and only the UE position is estimated. The SPEB for each case was derived as a function of the ideal case SPEB: no UE or BS clock biases. Relationships between the SPEB of the three studied cases were also established. The main takeaway from the SPEB analysis is that jointly estimating the UE's clock bias and position does not necessarily yield a better positioning performance compared to estimating the UE position only, even when the UE clock bias statistics are unknown. The cdf of the SPEB for each case was evaluated numerically using stochastic geometry models. Monte Carlo simulations were presented to demonstrate the SPEB relationships between the three cases.

References

[1] *Wireless E911 Location Accuracy Requirements*, Federal Commun. Comm., Washington, DC, USA, Feb. 2015. [Online]. Available: https://apps.fcc.gov/edocspublic/attachmatch/FCC-15-9A1

[2] C. Gentner, E. Munoz, M. Khider, E. Staudinger, S. Sand, and A. Dammann, "Particle filter based positioning with 3GPP-LTE in indoor environments," in *Proc. IEEE/ION Position Location Navig. Symp.*, Apr. 2012, pp. 301–308.

[3] Z. Z. M. Kassas, J. Khalife, K. Shamaei, and J. Morales, "I hear, therefore I know where I am: Compensating for GNSS limitations with cellular signals," *IEEE Signal Process. Mag.*, vol. 34, no. 5, pp. 111–124, Sep. 2017.

[4] M. Maaref, J. Khalife, and Z. M. Kassas, "Lane-level localization and mapping in GNSS-challenged environments by fusing lidar data and cellular pseudoranges," *IEEE Trans. Intell. Veh.*, vol. 4, no. 1, pp. 73–89, Mar. 2019.

[5] J. Khalife and Z. M. Kassas, "Precise UAV navigation with cellular carrier phase measurements," in *Proc. IEEE/ION Position Location Navig. Symp.*, Apr. 2018, pp. 978–989.

[6] K. Shamaei and Z. M. Kassas, "Sub-meter accurate UAV navigation and cycle slip detection with LTE carrier phase," in *Proc. ION GNSS Conf.*, Sep. 2019, pp. 2469–2479.

[7] J. Khalife and Z. M. Kassas, "Navigation with cellular CDMA signals—Part II: Performance analysis and experimental results," *IEEE Trans. Signal Process.*, vol. 66, no. 8, pp. 2204–2218, Apr. 2018.

[8] C. Yang, T. Nguyen, and E. Blasch, "Mobile positioning via fusion of mixed signals of opportunity," *IEEE Aerosp. Electron. Syst. Mag.*, vol. 29, no. 4, pp. 34–46, Apr. 2014.

[9] M. Driusso, C. Marshall, M. Sabathy, F. Knutti, H. Mathis, and F. Babich, "Indoor positioning using LTE signals," in *Proc. Int. Conf. Indoor Positioning Indoor Navig.*, Oct. 2016, pp. 1–8.

[10] K. Shamaei, J. Khalife, and Z. M. Kassas, "Exploiting LTE signals for navigation: Theory to implementation," *IEEE Trans. Wireless Commun.*, vol. 17, no. 4, pp. 2173–2189, Apr. 2018.

[11] J. Khalife and Z. M. Kassas, "Opportunistic UAV navigation with carrier phase measurements from asynchronous cellular signals," *IEEE Trans. Aerosp. Electron. Syst.*, early access, Oct. 25, 2019, doi: 10.1109/TAES.2019.2948452.

[12] M. Haenggi, J. G. Andrews, F. Baccelli, O. Dousse, and M. Franceschetti, "Stochastic geometry and random graphs for the analysis and design of wireless networks," *IEEE J. Sel. Areas Commun.*, vol. 27, no. 7, pp. 1029–1046, Sep. 2009.

[13] J. G. Andrews, F. Baccelli, and R. K. Ganti, "A tractable approach to coverage and rate in cellular networks," *IEEE Trans. Commun.*, vol. 59, no. 11, pp. 3122–3134, Nov. 2011.

[14] J. Schloemann, H. S. Dhillon, and R. M. Buehrer, "Toward a tractable analysis of localization fundamentals in cellular networks," *IEEE Trans. Wireless Commun.*, vol. 15, no. 3, pp. 1768–1782, Mar. 2016.

[15] S. Aditya, A. F. Molisch, and H. M. Behairy, "A survey on the impact of multipath on wideband time-of-arrival based localization," *Proc. IEEE*, vol. 106, no. 7, pp. 1183–1203, Jul. 2018.

[16] C. E. O'Lone, H. S. Dhillon, and R. M. Buehrer, "A statistical characterization of localization performance in wireless networks," *IEEE Trans. Wireless Commun.*, vol. 17, no. 9, pp. 5841–5856, Sep. 2018.

[17] S. Aditya, H. S. Dhillon, A. F. Molisch, R. M. Buehrer, and H. Behairy, "Characterizing the impact of SNR heterogeneity on time-of-arrival-based localization outage probability," *IEEE Trans. Wireless Commun.*, vol. 18, no. 1, pp. 637–649, Jan. 2019.

[18] Y. Shen and M. Z. Win, "Fundamental limits of wideband localization—Part I: A general framework," *IEEE Trans. Inf. Theory*, vol. 56, no. 10, pp. 4956–4980, Oct. 2010.

[19] Z. Liu, F. Meyer, and M. Z. Win, "On the accuracy of network localization and synchronization," in *Proc. Latin Amer. Conf. Commun. (LATINCOM)*, Nov. 2018, pp. 1–6.

[20] M. Z. Win, Y. Shen, and W. Dai, "A theoretical foundation of network localization and navigation," *Proc. IEEE*, vol. 106, no. 7, pp. 1136–1165, Jul. 2018.

[21] *Evolved Universal Terrestrial Radio Access (E-UTRA); Requirements for Support of Radio Resource Management*, 3GPP Standard TS 36.133, Apr. 2010.